energies

MDPI

Article

Combustion Analysis of Homogeneous Charge Compression Ignition in a Motorcycle Engine Using a Dual-Fuel with Exhaust Gas Recirculation

Yuh-Yih Wu [1,*] and Ching-Tzan Jang [1,2]

1 Department of Vehicle Engineering, National Taipei University of Technology, Taipei 10608, Taiwan; edward.ct.jang@gmail.com

2 Giant Lion Know-How Co., Ltd., Taipei 10692, Taiwan

* Correspondence: cyywu@ntut.edu.tw; Tel.: +886-2-2771-2171 (ext. 3620)

Received: 25 January 2019; Accepted: 25 February 2019; Published: 4 March 2019

Abstract: Exhaust emissions from the large population of motorcycles are a major issue in Asian countries. The regulation of exhaust emissions is therefore becoming increasingly stringent, with those relating to nitrogen oxides (NO_x) the most difficult to pass. The homogeneous charge compression ignition (HCCI) has special combustion characteristics and hence produces low NO_x emissions and exhibits high thermal efficiency. This study developed an HCCI system for a 150 cc motorcycle engine. The target engine was modified using a dual-fuel of dimethyl ether (DME) and gasoline with exhaust gas recirculation (EGR). It was tested at 2000–4000 rpm and the analysis was focused on 2000 rpm. The DME was supplied continuously at an injection pressure of 1.5 kg/cm^2. The gasoline injection rate was adjusted at a pressure of 2.5 kg/cm^2. A brake-specific fuel consumption of <250 g/kW·h was achieved under a condition of air–fuel equivalence ratio (λ) < 2 and an EGR of 25%. The nitric oxide concentration was too low to measure. The brake mean effective pressure (BMEP) increased by 65.8% from 2.93 to 4.86 bar when the EGR was 0% to 25%. The combustion efficiency was close to 100% when the BMEP was >3 bar.

Keywords: homogeneous charge compression ignition (HCCI); exhaust gas recirculation (EGR); dual-fuel; dimethyl ether (DME); exhaust emission

1. Introduction

The number of motorcycles in Asia is extremely large. This is because motorcycles are low in cost and small in size, allowing freedom of movement in crowded areas, easy parking, and high mobility. For example, the density of motorcycles in Taiwan in 2018 was 384/km^2 [1], the highest in the world. Motorcycles contribute to air pollution more than other vehicles [2,3]. They not only damage human health but also contribute to global warming. Consequently, regulations on their exhaust emissions and fuel consumption are becoming more stringent.

For instance, the Economic Commission of Europe (ECE) established long-term stage-by-stage emission regulations for motorcycles from 1999, as shown in Figure 1. The Taiwan Environmental Protection Administration (EPA) implemented motorcycle emission regulations from 1988, in a stage-by-stage approach. Taiwan's regulations were harmonized with ECE regulations from their fifth stage, which is similar to EURO 3 (i.e., the third stage of the ECE). The double-arrow red lines in Figure 1 link the corresponding stages between Taiwan and ECE. The implementation of Taiwanese regulations occurred approximately 1 year later than ECE regulations.

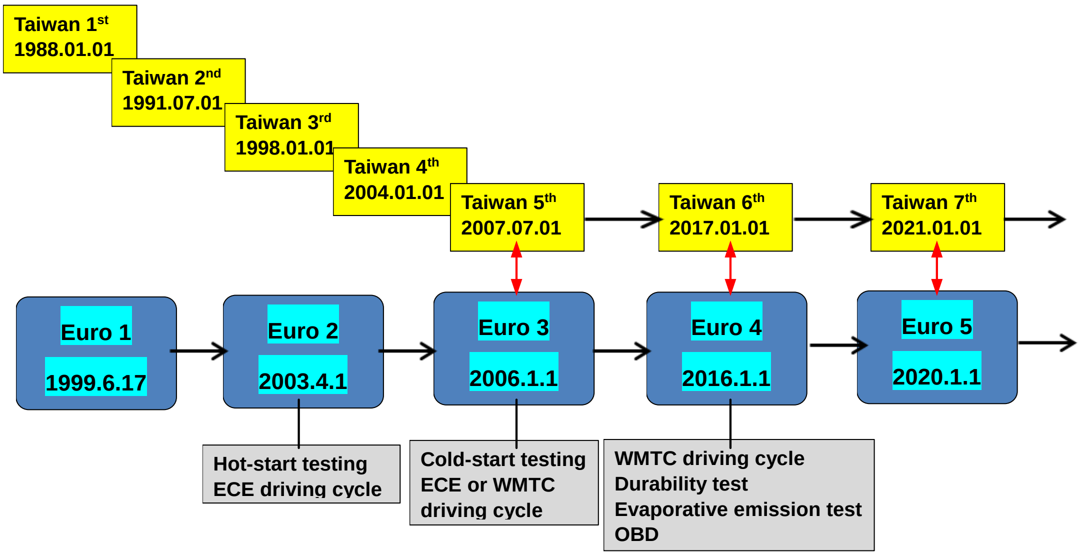

Figure 1. Evolution of motorcycle emission regulations by the ECE and Taiwan (WMTC: worldwide motorcycle test cycle; OBD: on-board diagnostics).

Table 1 shows the current and next-stage emission standards for motorcycles in Taiwan [4]. This encompasses carbon monoxide (CO), hydrocarbons (HC), non-methane hydrocarbons (NMHC), nitrogen oxides (NO_x), and particulate matter (PM). The emission standards of the sixth and seventh stages in Table 1 are the same as those in EURO 4 and 5, respectively. Numerous Asian countries follow the ECE regulations. To comply with emission standards, all the motorcycles produced in Taiwan now use an electronic fuel injection system. The NO_x standard is the most difficult to pass. In-use motorcycles emission controlled by Taiwan's EPA have even been recalled because of high NO_x emissions. Although lean-burn can improve fuel economy, motorcycle manufacturers do not use this approach. This is because NO_x emissions are difficult to reduce in a lean-burn system. The seventh-stage standard will be implemented from 1 January 2021. This will be extremely strict, which means that new technologies must be developed.

Table 1. Emission standards of motorcycles in Taiwan.

Stage (Implemented Date)	Maxi. Speed (km/h)	CO (mg/km)	HC (mg/km)	NMHC (mg/km)	NO_x (mg/km)	PM [1] (mg/km)
6th stage (1 Jan. 2017)	<130 ≥130	1140 1140	380 170	- -	70 90	- -
7th stage (1 Jan. 2021)	-	1000	100	68	60	4.5

[1] Particulate matter (PM) is for gasoline direct injection engines only.

In a spark ignition (SI) engine, a three-way catalytic converter efficiently reduces HC, CO, and NO_x, although the mixture must be maintained within a narrow air-fuel-ratio window. Other technologies for reducing NO_x include exhaust gas recirculation (EGR) [5], selective catalytic reduction (SCR) [6], a NO_x trap [7], a plasma reactor [8], water injection [9], water/fuel emulsions [10], and homogeneous charge compression ignition (HCCI) [11–13]. SCR and lean NO_x-trap have been applied in diesel vehicles to meet standard emission limits [14]. However, these systems increase production costs and cannot be used in motorcycles. An HCCI engine has special characteristics, as it constitutes a combination of an SI engine and a diesel engine. The homogeneous charge of fuel–air mixture is similar to that in an SI engine, whereas the compression ignition is similar to that in a diesel engine. Such combustion characteristics produce very low amounts of NO_x emissions and exhibit high thermal efficiency.

HCCI is an advanced low-temperature combustion concept that has attracted global attention in recent years [12]. However, the operational range of HCCI combustion is restricted due to the absence of direct control of the ignition timing and heat release rate [15]. In short, the key issues affecting HCCI combustion are thermal effects and chemical kinetics.

The factors that cause thermal effects include negative valve overlap (NVO), intake heating, glow plug, spark-assisted combustion, and compression ratio. NVO engines retain hot residual gas in the cylinder to heat the intake charge, extending the engine load range [16]. The intake heating improves autoignition, advances the combustion phase, and shortens combustion duration [15]. Spark-assisted HCCI reduces combustion noise under high-load conditions [17,18] and extends the operating load up to 750 kPa indicated mean effective pressure (IMEP) [18]. The glow plug can be used to control the heat release rate, and the temperature distribution is broadened to heat the charge unevenly [19]. A suitable compression ratio is necessary, which is from 12 to 18 according to most studies on HCCI engines.

The factors that cause the chemical kinetic effect include fuel composition, fuel properties, dual-fuel, external EGR, EGR stratification, and fuel stratification. One of the vital properties of fuel used for HCCI is its autoignition temperature. Fuel with a low autoignition temperature is termed diesel-like fuel and fuel with a high autoignition temperature is called gasoline-like fuel. To ensure suitable ignition timing and combustion phasing, an additive fuel is used. Diesel-like fuel can be used as an additive to enhance autoignition in a gasoline-like fuel system. Gasoline-like fuel can also be used as an additive to inhibit autoignition in a diesel-like fuel system.

Ji et al. [20] used a diesel-like fuel of 2-ethylhexyl nitrate to enhance the autoignition of an E10 gasoline HCCI engine. A maximum indicated thermal efficiency of 50.1% was found at 1800 rpm and an intake pressure of 180 kPa. Wang et al. [21] developed a DME-diesel blend fuel system using the gasoline-like fuel of liquefied petroleum gas as an ignition inhibitor. Pedersen et al. [22] used the port fuel injection (PFI) of methanol in the direct injection (DI) of a DME engine. The added methanol increased the BMEP and slowed the combustion so that it was after top dead center (aTDC). Mohebbi et al. [14] applied a PFI of ethanol and diethyl-ether blend fuel in a DI diesel engine: this resulted in a 14% increase in IMEP and a 33% reduction in the maximum rate of pressure rise (MRPR). Li et al. [23] investigated a blend of n-butanol and n-heptane in HCCI combustion and found that the knock tendency decreased as the n-butanol volume fraction increased. Khandal et al. [24] used a PFI of hydrogen in the DI of a biodiesel engine, which resulted in 65%–67% less smoke and 98%–99% lower NO_x emissions. Finally, Zheng et al. [25] developed a dual-fuel system using the DI of biodiesel and PFI of several gasoline-like fuels. Among the gasoline-like fuels, the biodiesel-ethanol produced low NO_x and soot emissions (soot < 0.3 FSN and NO_x < 1.5 g/kW·h).

Regarding the mechanism of the effect of EGR on combustion, the addition of EGR slows the decomposition of hydrogen peroxide (H_2O_2) by reducing the rate of hydroxyl radicals (OH) [26]. This results in the suppression of autoignition and delay of combustion phasing, thus allowing high load operation. Researchers [27,28] have reported that in-cylinder EGR stratification reduced the MRPR of HCCI engines. Other researchers [13,29] have reported that the effects of external EGR on HCCI engines were a delay in combustion phasing, decrease in maximum temperature and maximum HRR (heat release rate), prolonged high-temperature heat release, and decreased MRPR. Lee et al. [30] investigated the optimization of EGR (0–25%) and two-stage injection with compression ratios of 15 and 17.8.

Superior HCCI operation can be achieved using a combination of several strategies, such as the stratification of external EGR, fuel stratification using PFI and DI injectors including asymmetric injection, open valve injection using a PFI injector, and NVO injection [31]. Researchers [16,32] have developed an HCCI engine with intake boosting, NVO, and external EGR. The engine load was extended to an IMEP of 8 bar. This type of system can achieve a thermal efficiency of 47%, NO_x of $\leq$0.1 g/kW·h, and combustion efficiency of $\geq$96.5% [16].

The best elements of previous research have been developed for automobile engines and cannot be used for motorcycles. Most motorcycle engines are small-scale, with a displacement $\leq$150 cc, while the surface-volume ratio is large compared to automobile engines and hence causes high heat loss [33]. This condition makes HCCI operation in motorcycles difficult. Additionally, the combustion characteristics of a small-scale air-cooled HCCI engine are insufficient. Therefore, a combination of DME-gasoline dual-fuel and external EGR with a suitable compression ratio for HCCI operation was developed. This is useful for low-cost motorcycle engines with only minor modifications. The purpose of this study was to therefore investigate the combustion characteristics of this HCCI system.

2. Experimental Methodology

2.1. Experimental Setup

A commercial motorcycle engine (SYM, Taipei, Taiwan) with an electronic fuel injection system was retrofitted for HCCI operation. The engine was a 150 cc air-cooled SI engine. Detailed engine specifications are listed in Table 2. The compression ratio was increased from 10.5 to 12.4 by replacing the cylinder head with a smaller clearance volume. The increased compression ratio raises the temperature of the compressed mixture, which easily achieves compression ignition.

Table 2. Engine specifications.

Items	Specifications	Units
Engine type	4-stroke, 1-cylinder, SI	-
Valve system	4-valve, overhead cam	-
Cooling system	Forced air cooling	-
Displacement	150	cc
Bore × stroke	57.4 × 57.8	mm
Compression ratio	10.5 changed to 12.4	-
Fuel system	Electronic port fuel injection	-
Intake valve open [1]	10° bTDC	CA
Intake valve close [1]	20° aBDC	CA
Exhaust valve open [1]	30° bBDC	CA
Exhaust valve close [1]	10° aTDC	CA

[1] Valve timing is defined at 1 mm of valve lift. aTDC: after top dead center; bTDC: before top dead center; aBDC: after bottom dead center; bBDC: before bottom dead center.

The fuel for HCCI operation in an SI engine should have a low autoignition temperature. Previous research [34] has concluded that DME, the properties of which are listed in Table 3, is a favorable choice for this. The cetane number of DME is 60, higher than that of diesel fuel (i.e., 40–60). It can autoignite in the target engine. Therefore, DME was selected as the main fuel. Increasing the fuel amount of DME to increase engine load will cause high MRPR or engine knocking.

Table 3. Fuel properties.

Properties	DME	Gasoline
Chemical structure	C_2H_6O	-
Lower heating value (MJ/kg)	28.9	44.0
Octane number	35	92
Cetane number	60	5–12
Autoignition temperature [1] (K)	508	553–729
Stoichiometric air-fuel ratio	9.0	14.7
Viscosity at 20 °C (cP)	0.224	0.74

[1] Autoignition temperatures were obtained from Material Safety Data Sheets.

Gasoline with a research octane number (RON) 92 and external EGR were added to extend the operating range of the engine. The autoignition temperature of gasoline is much higher than that of DME, as shown in Table 3. The addition of gasoline can therefore increase the engine load without knocking.

The experimental setup for the proposed HCCI engine is shown in Figure 2. The external EGR system was built on the target engine with a small EGR pump and a control valve, which adjusted the EGR ratio. A surge tank was installed between the air flow meter and the throttle; it was used for attenuating the pressure pulsation in the intake system of the engine. So the intake air flow rate can be measured stably. The volume of the surge tank is 40 L, which is larger than the minimum requirement calculated according to SAE J244. A dual-fuel supplying system was then built into the target engine (Figure 3). The original fuel and ignition systems of the target engine were retained to start the engine. The spark plug was used only for starting the engine and the spark timing was the same as the original engine. The original gasoline injector was also used for the addition of gasoline in the HCCI engine. The additional DME supplying system, which includes a DME tank, pressure regulator, filter, and a flow meter, was attached to the target engine with a DME supply tube installed near the intake port.

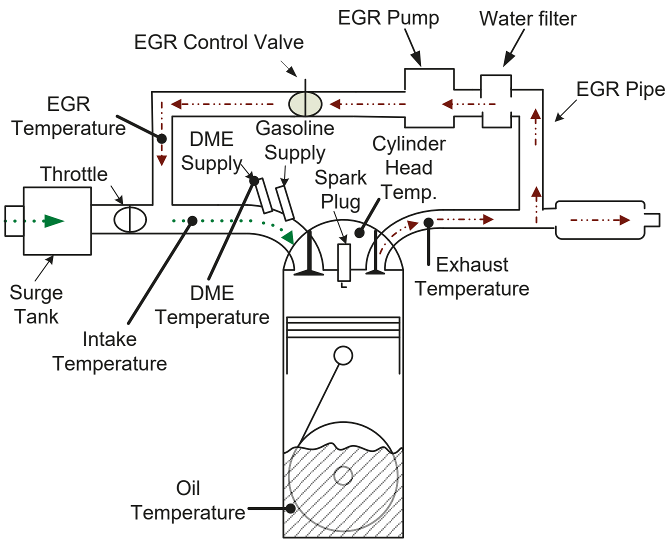

Figure 2. Experimental setup for the proposed dual-fuel HCCI engine with external EGR.

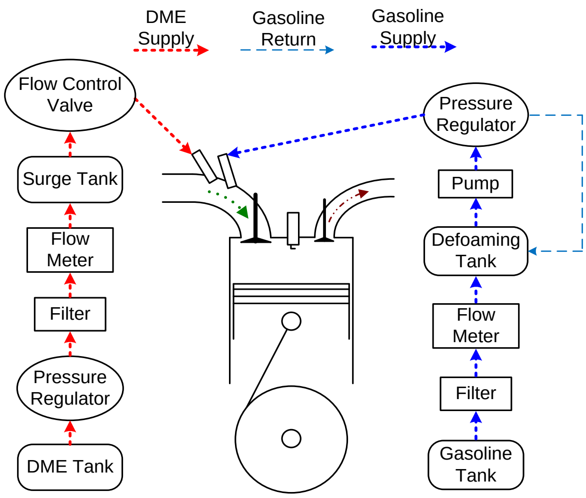

Figure 3. Experimental setup for the fuel supply system.

For the engine test, an eddy-current engine dynamometer (FE150-S, Borghi & Saveri S.R.L., Bologna, Italy) was used to measure the engine speed and brake torque. The gasoline flow rate was measured using a mass burette flow detector (FX-1110, Ono Sokki, Yokohama, Japan). The DME flow rate was measured using a thermal mass flow controller (NM-2100, Tokyo Keiso, Tokyo, Japan). The exhaust emissions of CO, HC, NO, carbon dioxide (CO_2), oxygen, and the lambda were measured using an emission analyzer (MEXA-584L, Horiba, Kyoto, Japan). The lambda is calculated by the carbon balance method in standard configuration using the MEXA-584L emission analyzer. The hydrogen/carbon ratio and oxygen/carbon ratio of the fuel must be input to this analyzer. Additionally, another emission analyzer (MEXA-584L, Horiba) was installed in the intake system to measure the CO_2 concentration and thus calculate the EGR ratio. K-type thermocouples were installed on the engine to measure the temperature of the intake gas, exhaust gas, cylinder head, and lubricating oil, as shown in Figure 2.

A piezoelectric pressure transducer (Kistler 6051B, Winterthur, Switzerland) coupled to a charge amplifier (Kistler 5018A) was used to record in-cylinder gas pressure. A shaft encoder (BEI H25, Thousand Oaks, CA, USA) was used to detect the crank angle (CA). The pressure signal was transmitted to a data acquisition system (IndiCom 619, AVL, Graz, Austria) for every 1 °CA of 100 continuous cycles. The number of cylinder pressure data of 100 cycles is good enough for the combustion analysis. The pressure data were used to analyze engine combustion parameters, such as the in-cylinder gas temperature, coefficient of variation (COV), and HRR.

The engine control was replaced by a controller (MotoHawk ECU 555-80, Woodward, CO, USA) which controlled the spark timing (for SI engine starting), gasoline injector, DME flow control valve, and EGR control valve.

Temperature is an important factor in HCCI engines [35]. Reference [36] has shown that, for stable HCCI operation in a small engine the cylinder head and oil temperatures should be maintained above 120 °C and 65 °C, respectively. The intake charge temperature of all tests in this research ranges from 21.2 °C to 23.2 °C, its mean value is 22.4 °C, and the standard deviation is 0.6 °C. The range of intake temperature is not large, so the influence of intake temperature on combustion can be neglected.

The engine was started using the original ignition and fuel systems. When the cylinder head and oil temperatures reached 120 °C and 65 °C, respectively, the controller switched the engine operation to HCCI mode by interrupting the ignition system. Simultaneously, the dual-fuel of DME and gasoline was injected and the throttle was opened further. The throttle was used only for SI operation of the original engine. For HCCI operation, it was fully opened. The fuel supply was adjusted for stable HCCI operation; the ratio of these two fuels was therefore not fixed. The engine was tested at 2000–4000 rpm and with a wide-open throttle. Most of the analyses were focused on 2000 rpm because its operating load range was large. The DME fuel was supplied continuously; its injection pressure was adjusted before engine test for stable combustion and it was found to be 1.5 kg/cm^2. The gasoline was injected at a pressure of 2.5 kg/cm^2, which was the same as the original engine. The gasoline fuel injection pulse width was adjusted to set the fuel flow rate. The EGR ratio was adjusted from 0% to 30%.

The engine speed, brake torque, DME flow rate, gasoline flow rate, intake air mass flow rate, exhaust emissions, and EGR ratio were measured and recorded during the engine tests. The EGR ratio was calculated using the CO_2 percentages measured in the intake and exhaust systems, as formulated in Equation (1) [37]:

$$EGR = \frac{[CO_2]_{in}}{[CO_2]_{exh}} \times 100\%, \tag{1}$$

where $[CO_2]$ is the CO_2 concentration.

The maximum error of the experimental data was calculated with an engine test at 2000 rpm and repeated five times using the Kline and McClintock method [38]. The results are listed in Table 4.

Table 4. Maximum error in the experimental results of the engine test.

Item	Maximum Error (± %)
Engine Speed	0.68
Engine Torque	1.75
IMEP	1.92
Fuel Rate	5.57

2.2. Calculation of Combustion Parameters

Combustion parameters, such as IMEP, COV, combustion efficiency, cylinder gas temperature, HRR, and MFB, are used to study the combustion characteristics of an engine.

IMEP is defined as the work divided by the engine displacement volume, which can be calculated during compression and expansion strokes without pumping work. Because this study focused on combustion effect, the elimination of intake and exhaust strokes is better for analyzing. This is expressed as:

$$IMEP = \frac{\int_{-180CAD}^{180CAD} PdV}{V_d}, \tag{2}$$

where CAD denotes CA degrees.

The COV is expressed as:

$$COV = \frac{IMEP_{std}}{IMEP_{avg}}, \tag{3}$$

The combustion efficiency η_c can be defined as the fraction of carbon emitted as CO_2 in relation to the total carbon emitted (CO_2, CO, HC and PM). The modified combustion efficiency is defined as the ratio between CO_2 and CO_2 plus CO. This study used the modified combustion efficiency for convenient calculation. This is expressed as:

$$\eta_c = \frac{[CO_2]}{[CO_2] + [CO]}, \tag{4}$$

where square bracket [ ] represents exhaust species concentration as a percentage.

The in-cylinder gas temperature is obtained using the state equation of ideal gas. The HRR equation can be derived from the first law of thermodynamics and is thus expressed as:

$$\frac{dQ_{hr}}{d\theta} = \frac{\gamma}{\gamma - 1} p \frac{dV}{d\theta} + \frac{1}{\gamma - 1} V \frac{dp}{d\theta} + \frac{dQ_{ht}}{d\theta}, \tag{5}$$

where $dQ_{hr}/d\theta$ is the HRR, $dQ_{ht}/d\theta$ is the heat transfer rate between cylinder gas and the wall. The specific heat ratio γ is a function of temperature, which can be obtained using the empirical equation presented in [39].

The heat transfer rate $dQ_{ht}/d\theta$ is expressed as:

$$\frac{dQ_{ht}}{d\theta} = hA(T_g - T_w), \tag{6}$$

where h is the heat transfer coefficient, as shown in Equation (7):

$$h = S_t \rho_g c_p (0.5C_m) \text{ and} \tag{7}$$

$$S_t = 0.718 \exp(-0.145C_m), \tag{8}$$

where S_t is the Stanton number and C_m the average piston speed. Equations (7) and (8) were proposed by [33] for small engines.

The MFB at any CA is calculated from HRR and is expressed as:

$$MFB = \frac{\int \left(\frac{dQ_{hr}}{d\theta} \right) d\theta}{m_f Q_{LHV}}. \tag{9}$$

3. Results and Discussion

The experimental results are presented in terms of the performances, efficiencies, exhaust emissions, and combustion characteristics of the target engine. The data in Sections 3.1–3.4 are all at 2000 rpm of engine speed.

3.1. Engine Performances

The BMEP, IMEP, and brake-specific fuel consumption (BSFC) are discussed in this section. HCCI engines are always run with a lean mixture. Generally, the output of a HCCI engine increases with a richer mixture but is limited by engine knocking or MRPR [40]. The EGR is a kind of diluent in air-fuel mixture which suppresses the combustion rate. Previous research [41] has reported that autoignition timing is delayed and burn duration prolonged by applying EGR in a HCCI engine, which suppresses engine knocking. The test results for engine output with various EGR ratios are shown in Figure 4.

The BMEP and IMEP indicate the work output per cycle divided by the engine displacement volume. As shown in Figure 4, the engine output increases when the air–fuel equivalence ratio (lambda, λ) decreases. Each curve in Figure 4 indicates the operational range of each EGR ratio. The maximum engine output on each curve increases in line with the EGR. However, the EGR of 30% seems too high for this HCCI system because the operational range is very small and the engine output cannot be extended. In this study, an EGR of 25% yields the best engine output. When the EGR was increased from 0% to 25%, the maximum BMEP increased by 65.8% from 2.93 to 4.86 bar. In Figure 4, the first and last point of each EGR line were determined by the limit of stable operation, which is COV < 10% for low load and MRPR < 6 bar/deg for high load.

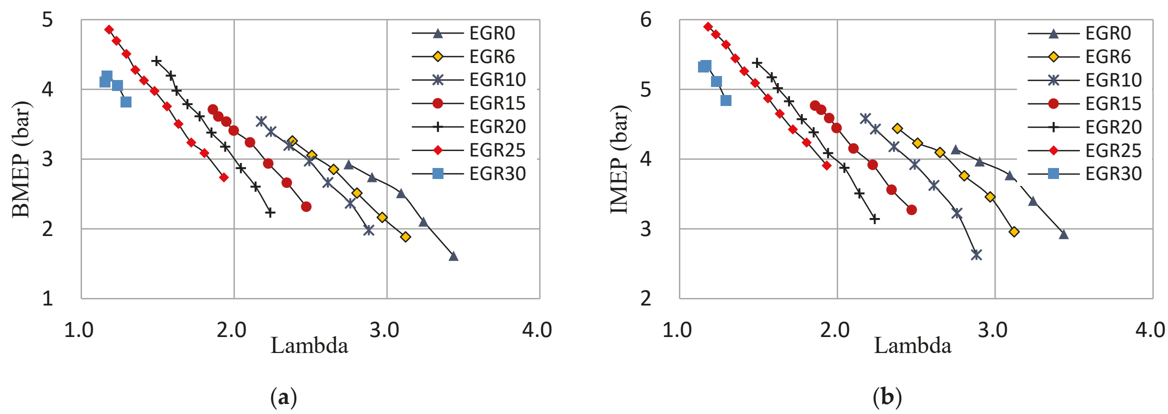

Figure 4. Effect of lambda on engine output with various EGR ratios: (**a**) BMEP; (**b**) IMEP.

Gasoline and DME were used in the dual-fuel system. DME was selected as the main fuel and was supplied at an almost constant flow rate. Increasing the gasoline mass ratio in the dual-fuel causes λ to decrease, as shown in Figure 5a. The BMEP increases in line with the amount of gasoline, as shown in Figure 5b. At an EGR of 25%, BMEP increases by 77.4% from 2.74 to 4.86 bar when the gasoline ratio rises from 0.13 to 0.35.

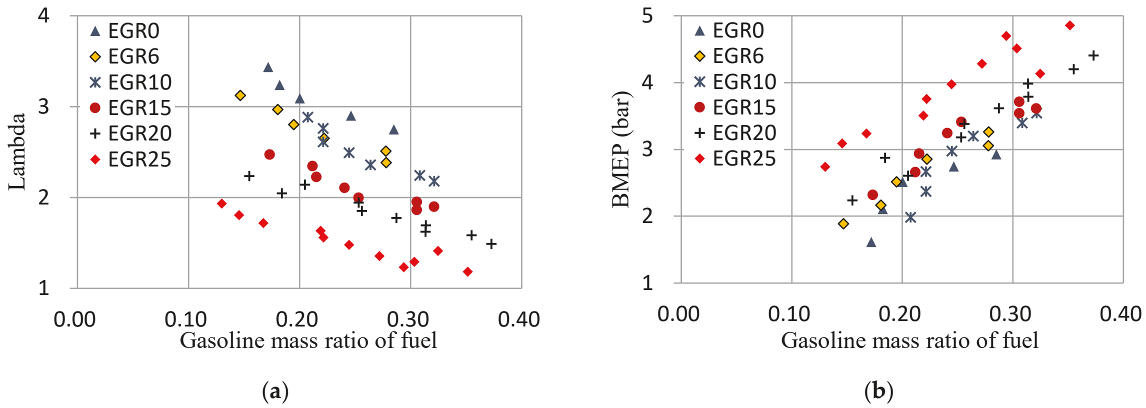

Figure 5. Effect of gasoline mass ratio in the dual-fuel on: (**a**) Lambda; (**b**) BMEP.

The fuel consumed contains gasoline and DME; therefore, an equivalent fuel mass was used. The equivalent fuel flow rate was calculated based on the heating value of the fuels, as shown in Equation (10), and the *BSFC* was calculated using Equation (11):

$$\dot{m}_e = \frac{\dot{m}_{DME} Q_{LHV\ DME} + \dot{m}_{gasoline} Q_{LHV}}{Q_{LHV}} \text{ and} \tag{10}$$

$$BSFC = \frac{\dot{m}_e}{bhp}, \tag{11}$$

where $\dot{m}_e$ is the fuel flow rate equivalent to gasoline, $\dot{m}_{DME}$ is DME flow rate, $\dot{m}_{gasoline}$ is gasoline flow rate, $Q_{LHV\ DME}$ is the low heating value of DME, Q_{LHV} is the low heating value of gasoline, and bhp is the brake horsepower.

Figure 6 shows the BSFC of all test points. Most of the operation conditions have a BSFC ranging from 230 to 260 g/kW·h. The BSFC of a HCCI engine is much lower than that of a conventional motorcycle engine, which is approximately 350 g/kW·h [42]. When λ is >2 or BMEP is <3 bar, the BSFC clearly increases. This might be caused by the low engine output and low combustion efficiency. A BSFC of ≤250 g/kW·h was achieved under conditions of λ < 2 and an EGR of 25%.

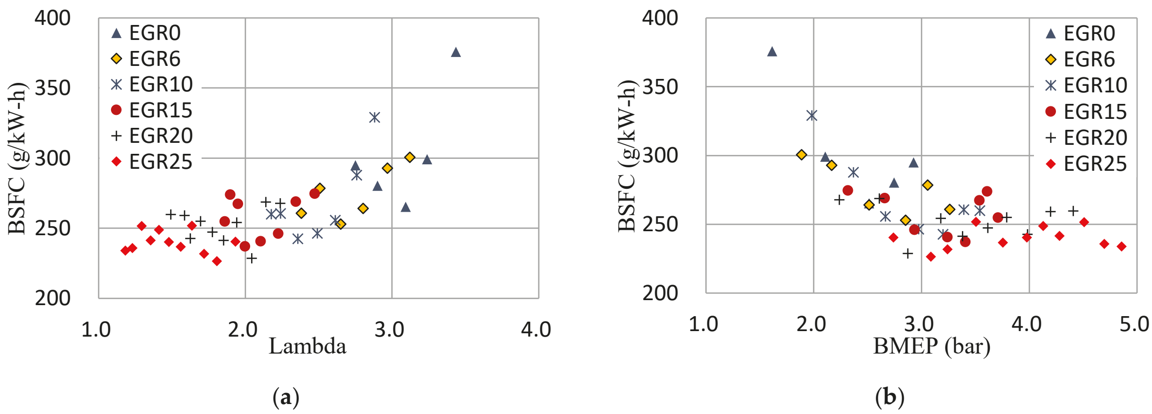

Figure 6. Brake specific fuel consumption with respect to: (**a**) Lambda; (**b**) BMEP.

3.2. Engine Efficiencies

The combustion efficiency, η_c, is the ratio of the fuel mass burned and the fuel mass delivered into the engine. It can be calculated using Equation (4). The fuel efficiency η_f is the ratio of the power developed by the engine to the rate of fuel energy in the engine. It is calculated using Equation (12):

$$\eta_f = \frac{bhp}{\dot{m}_f Q_{LHV}} = \frac{3600(s/h)}{BSFC(g/kW\cdot h)\cdot Q_{LHV}(kJ/g)}, \tag{12}$$

where bhp is the brake horsepower, $\dot{m}_f$ is the fuel flow rate, and Q_{LHV} the lower heating value of fuel.

The brake thermal efficiency η_{th} is calculated using Equation (13):

$$\eta_{th} = \frac{bhp}{\eta_c \dot{m}_f Q_{LHV}} = \frac{\eta_f}{\eta_c}, \tag{13}$$

Figure 7 shows that the combustion efficiency decreases with an increase in λ or decrease in engine load (BMEP) because a high λ or low BMEP leads to a leaner mixture and incomplete combustion. In Figure 7a, the effect of λ on combustion efficiency for each EGR ratio is separated each other and does not coincide together. However, the effect of BMEP on combustion efficiency is evident (Figure 7b), irrespective of the amount of EGR. The combustion efficiency was close to 100% when BMEP > 3 bar.

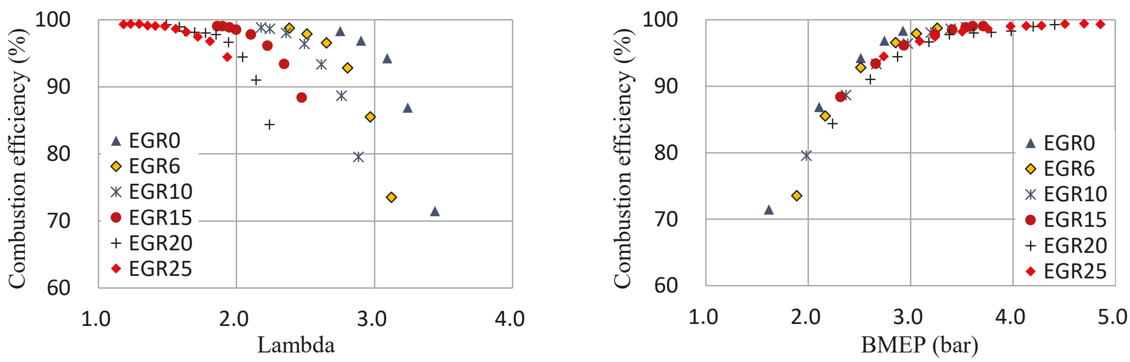

(**a**) (**b**)

Figure 7. Combustion efficiency with respect to: (**a**) Lambda; (**b**) BMEP.

Figure 8 shows that the fuel efficiency decreases with increasing λ or decreasing engine load (BMEP) because high λ or low BMEP leads to incomplete combustion. When λ is >2 or BMEP is <3 bar, the fuel efficiency clearly drops.

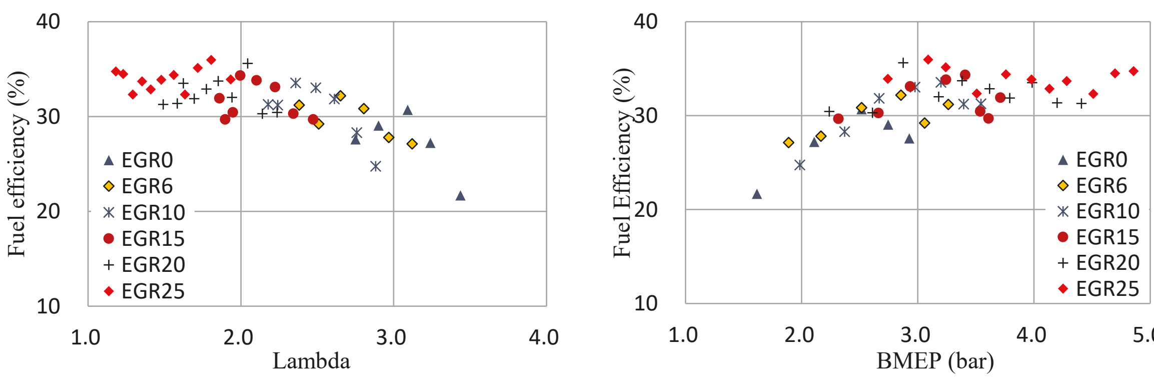

(**a**) (**b**)

Figure 8. Fuel efficiency with respect to: (**a**) Lambda; (**b**) BMEP.

The brake thermal efficiency is shown in Figure 9. Most of the brake thermal efficiencies are clustered within the range of 30%–35%. They have no clear relationship with λ or engine load (BMEP). The thermal efficiency is not very high because the target engine is small in size and heat loss is relatively high [33]. Furthermore, the HCCI engines do not require as much cooling as a conventional engine due to the low combustion temperature of HCCI. Therefore, the modification of a cooling system to reduce cooling capacity will be better for HCCI operation and will improve thermal efficiency.

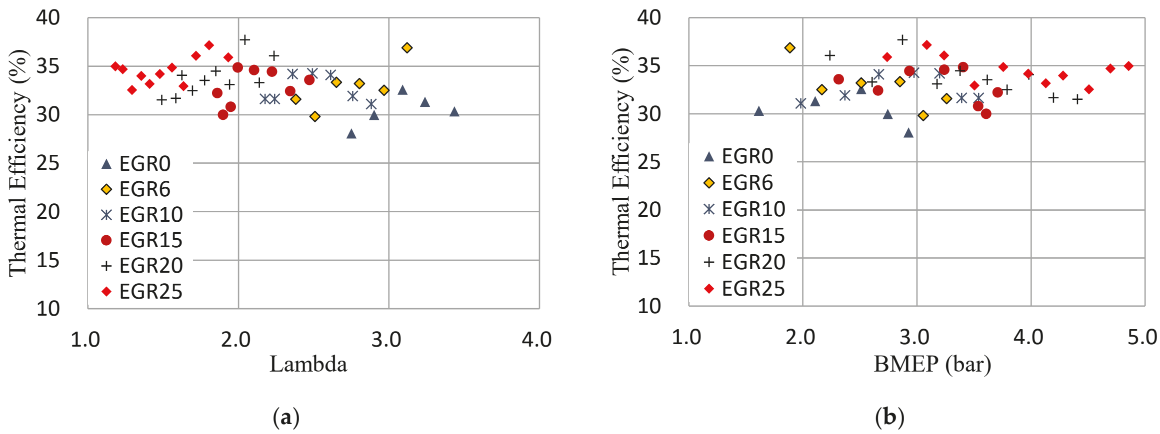

Figure 9. Brake thermal efficiency with respect to: (**a**) Lambda; (**b**) BMEP.

3.3. Exhaust Emissions

Emission data for NO is lacking because the concentration was too low to be measured during the engine test. In general, when the combustion temperature is lower than 1800 K, much less NO will be emitted [43]. The maximum cylinder temperatures of all test points in this study were less than 1600 K, which is much lower than 1800 K, so the NO emission was close to zero ppm.

The exhaust emissions of CO and HC are depicted through the brake-specific emissions as BSCO and BSHC. The BSCO increases with increasing λ or decreasing exhaust temperature, as shown in Figure 10. The leaner mixture causes higher CO emission in the HCCI engine (Figure 10a), which is the opposite of that in a conventional SI engine. The results obtained are in agreement with previous research [44,45]. This is because the combustion temperature of HCCI is lower and, again, will decrease with increasing λ. Sjöberg and Dec [44] reported that CO oxidation does not reach completion with a peak temperature below 1500 K because the OH level becomes too low.

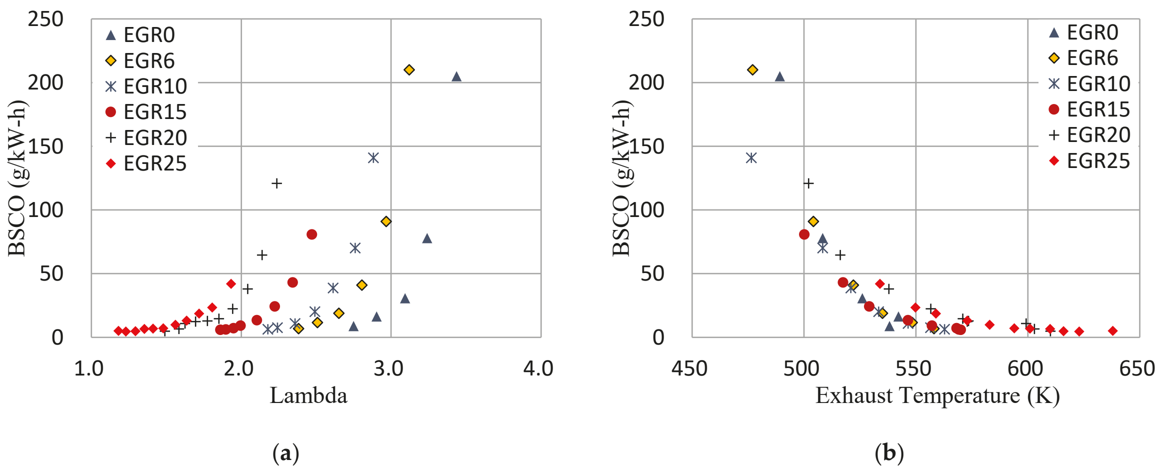

Figure 10. Brake specific CO emission with respect to: (**a**) Lambda; (**b**) Exhaust temperature.

In Figure 10a, the effect of λ on BSCO for each EGR ratio is separated each other and does not coincide together. However, the effect of exhaust temperature on BSCO is evident (Figure 10b), irrespective of the amount of EGR. The BSCO is close to 0 g/kW·h when the exhaust temperature is > 550 K.

The BSHC increases with increasing λ or decreasing exhaust temperature, as shown in Figure 11. A higher λ indicates a leaner mixture and leads to a lower combustion temperature, which causes an increase in HC emissions. Both BSCO and BSHC show good correlation with the exhaust temperature, but they do not correlate with the maximum cylinder gas temperature (the Figure for which is not included here). Thus, the high temperature of the exhaust gas results in the oxidation of CO and HC.

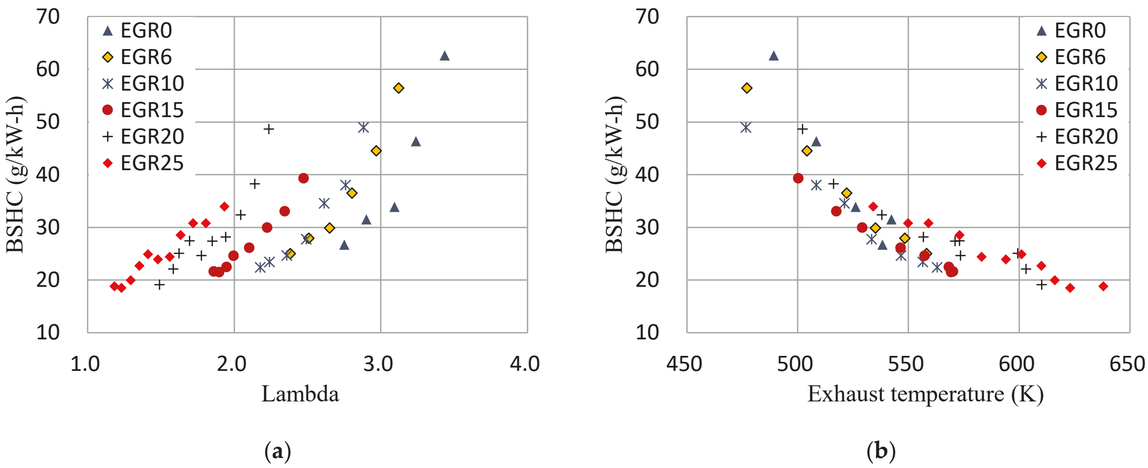

Figure 11. Brake specific HC emission with respect to: (**a**) Lambda; (**b**) Exhaust temperature.

The exhaust temperature increases in line with BMEP. The curve fitting of Figure 12a shows a good correlation between exhaust temperature and BMEP, with an R^2 of 0.9713. The oxygen concentration in the exhaust gas increases with λ as a quadratic equation, the R^2 of which is 0.9899 (Figure 12b).

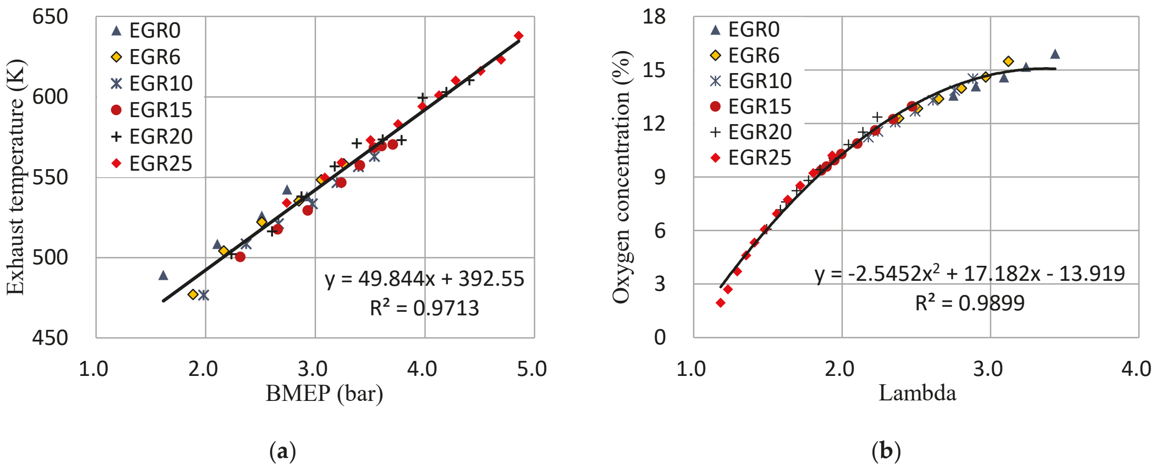

Figure 12. Curve fitting of exhaust properties: (**a**) Exhaust gas temperature versus BMEP; (**b**) Oxygen concentration in exhaust gas versus lambda.

3.4. Combustion Characteristics

The combustion characteristics were calculated from cylinder pressure values. The cylinder pressure and temperature under a condition of 25% EGR and 20% EGR with various λ values are illustrated in Figure 13. A lower λ means a large amount of gasoline is added, which delays the combustion phase and slows the onset of maximum cylinder pressure (Figure 13a,c). The cylinder temperature is very low (Figure 13b,d) compared with an SI engine because HCCI involves low-temperature combustion [12].

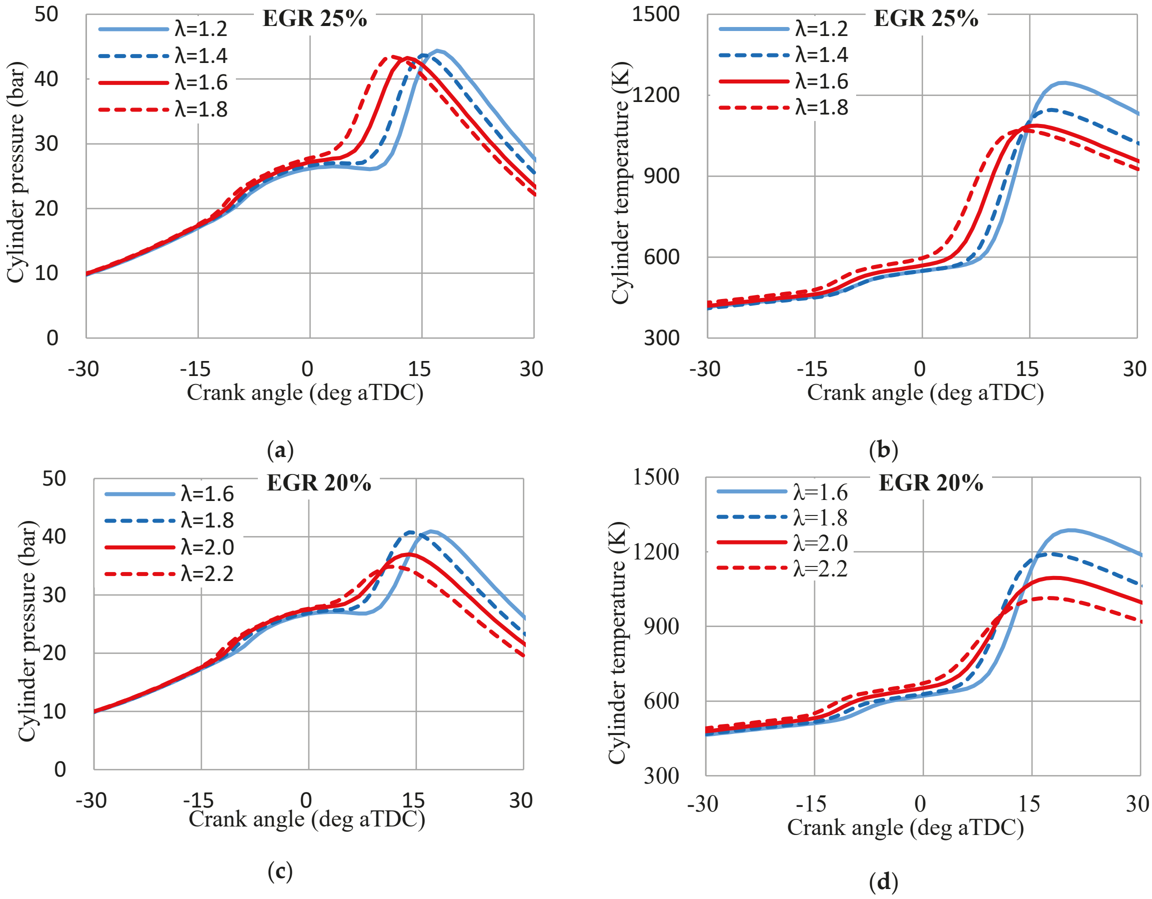

Figure 13. Cylinder pressure and temperature: (**a**) Cylinder pressure with EGR 25%; (**b**) Cylinder temperature with EGR 25%; (**c**) Cylinder pressure with EGR 20%; (**d**) Cylinder temperature with EGR 20%.

HRR and MFB under a condition of 25% EGR and 20% EGR with various λ values are illustrated in Figure 14. It is clear that the addition of more gasoline (less λ) causes higher HRR values and delays HRR and MFB. The beginning of the increase in HRR indicates the start of combustion. Figure 14a shows that the start of combustion is delayed by adding gasoline.

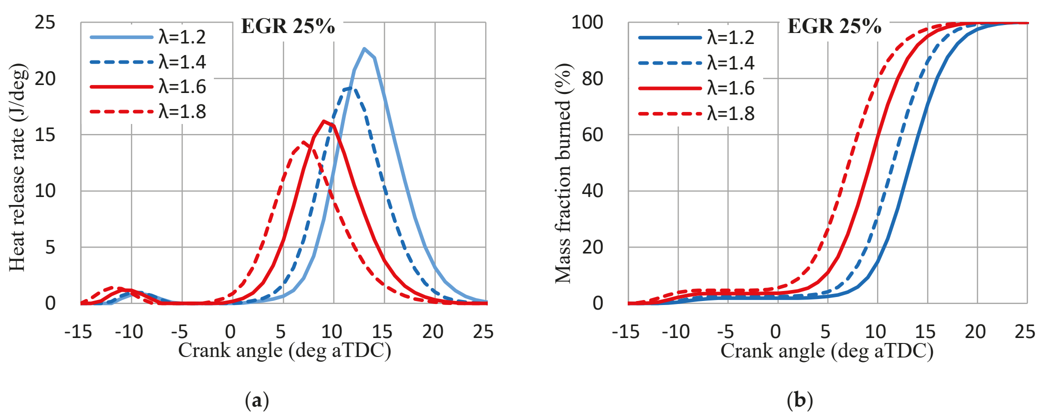

Figure 14. *Cont.*

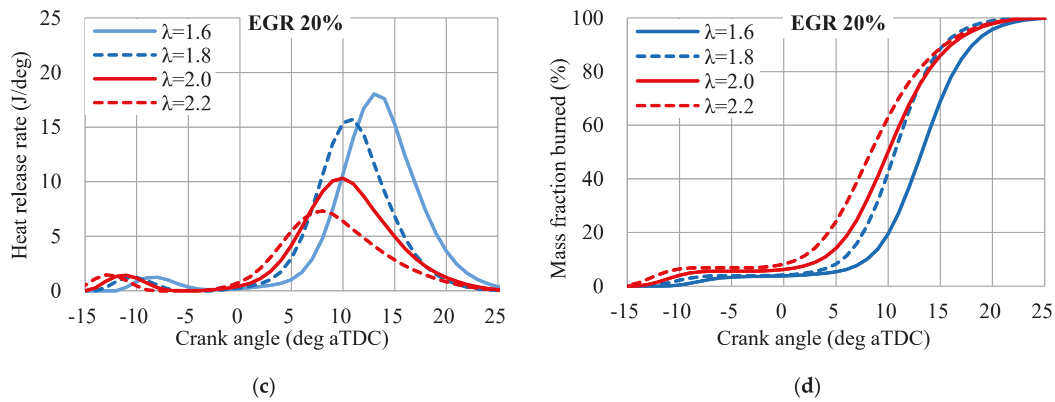

Figure 14. Heat release rate and mass fraction burned: (**a**) Heat release rate with EGR 25%; (**b**) Mass fraction burned with EGR 25%; (**c**) Heat release rate with EGR 20%; (**d**) Mass fraction burned with EGR 20%.

Figure 15 shows that COV decreases and MRPR increases with an increase in BMEP. The COV increases rapidly as BMEP is <3 bar (Figure 15a). In general, a low load causes unstable combustion and a high load causes a high rate of pressure rise or knocking [11,26]. Almost all the MRPR values are less than 6 bar/deg in Figure 15b, which is a criterion for avoiding engine damage [40]. This is because the addition of gasoline and EGR delays the ignition and suppresses the combustion reaction.

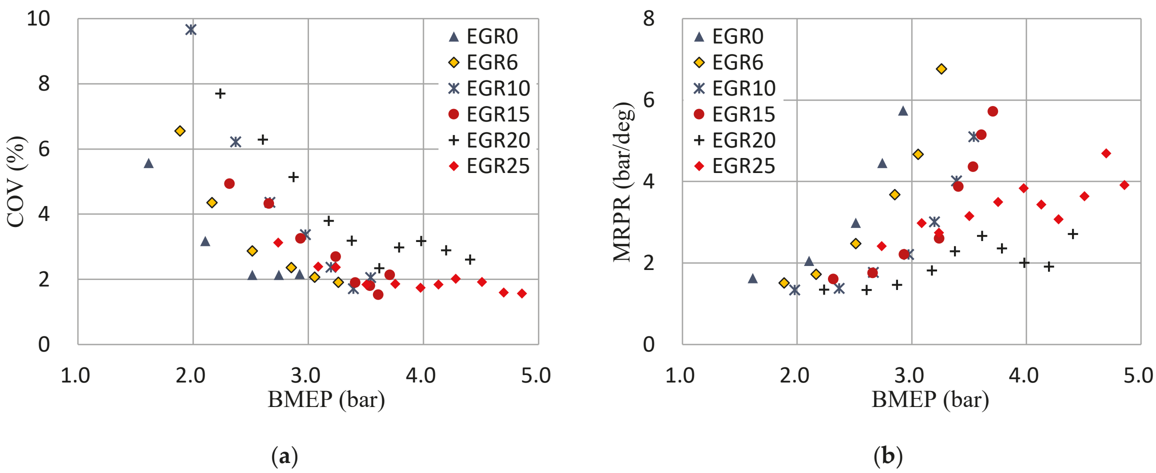

Figure 15. The coefficient of variation of IMEP (COV) and the maximum rate of pressure rise (MRPR) with respect to: (**a**) COV; (**b**) MRPR.

In Figure 16, the maximum HRR1 (first-stage HRR) increases with increasing λ, whereas maximum HRR2 (second-stage HRR) decreases with increasing λ. The first stage of combustion (Figure 16a) expresses the ignition property, whereas the second stage of combustion (Figure 16b) expresses the combustion property. The first stage of combustion is the result of cool-combustion chemistry and negative temperature coefficient behavior [46]. In the first stage of combustion, the reaction rate decreases after the temperature reaches a certain value. Therefore, the maximum HRR1 depends on λ only (Figure 16a). By contrast, the maximum HRR2 depends on both the λ value and EGR ratio (Figure 16b).

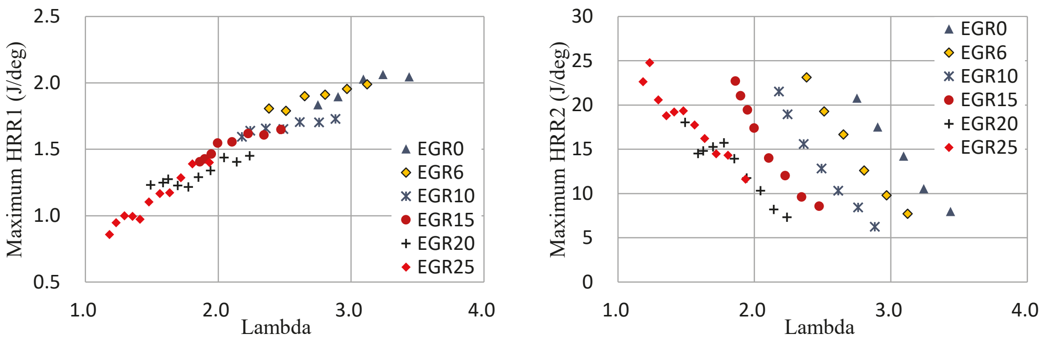

(**a**) (**b**)

Figure 16. Effects of lambda on maximum heat release rate: (**a**) First stage combustion, HRR1; (**b**) Second stage combustion, HRR2.

CA10, CA50, and CA90 are the CA values when MFB is 10%, 50%, and 90%, respectively. These indicate the combustion phase. Both CA10 and CA50 are delayed when λ is lower, as shown in Figure 17. This is caused by the effect of dual-fuel on combustion. A richer mixture (i.e., less λ) has much more gasoline (Figure 5a), which delays combustion. CA50 is a combination of first- and second-stage combustion, whereas CA10 represents first-stage combustion only. Therefore, the correlation between CA10 and λ (Figure 17a) is clearer than that of CA50 (Figure 17b).

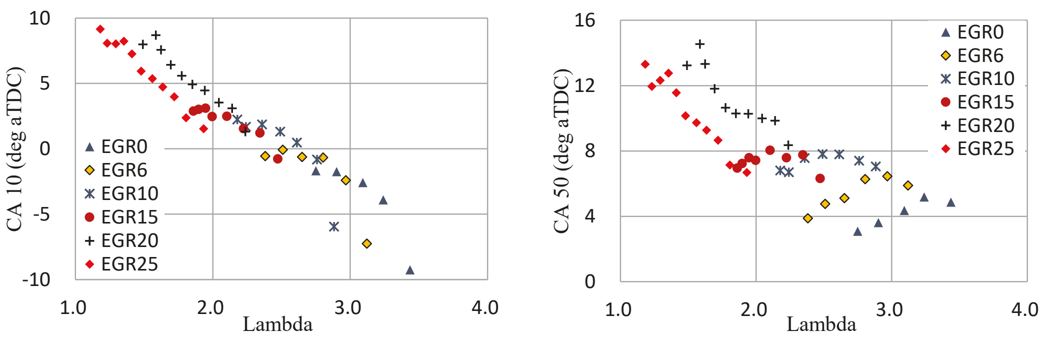

(**a**) (**b**)

Figure 17. Effects of lambda on combustion phasing: (**a**) CA10; (**b**) CA50.

Figure 18a shows that the burn duration (period between CA10 and CA90) increases with an increase in λ, because a leaner mixture causes slower combustion. Figure 18b shows that the burn duration increases rapidly when BMEP is <3 bar.

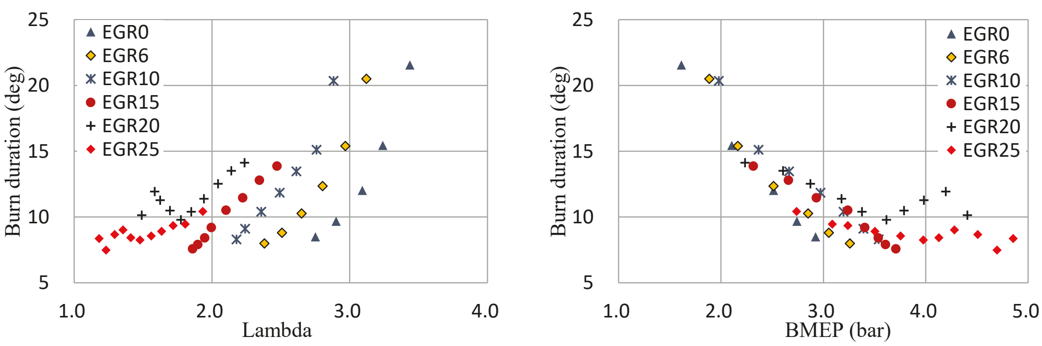

(**a**) (**b**)

Figure 18. Burn duration with respect to: (**a**) Lambda; (**b**) BMEP.

The combustion efficiency is close to 100% at a burn duration of <10 deg CA (Figure 19a), which equates to a BMEP of >3 bar (Figure 18b). The burn duration indicates the combustion rate, whereas CA10 indicates the start of combustion. Therefore, the influence of burn duration on the combustion efficiency is more obvious (Figure 19a) than in CA10 (Figure 19b).

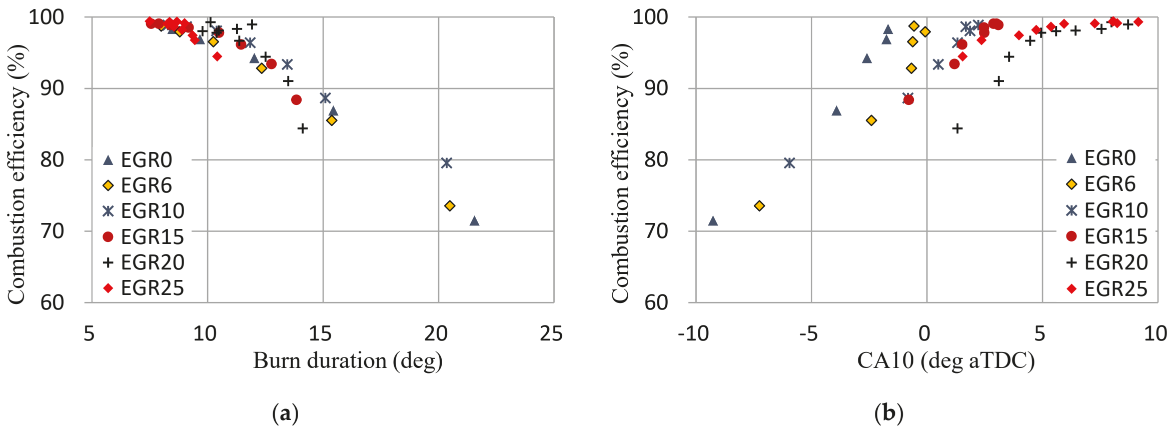

Figure 19. Combustion efficiency with respect to: (**a**) burn duration; (**b**) CA10.

3.5. Comparison between HCCI and SI

The engine speeds operated with HCCI contained 2000, 2600, 3000, 3300, 3500, and 4000 rpm. The experimental results of HCCI are compared with that of original SI engine as shown in Figures 20 and 21.

Figure 20a shows that the operating range of HCCI engine is much smaller than that of the original SI engine, so the proposed HCCI engine cannot be used in a conventional motorcycle. However, it could be used as a range extender for an electric motorcycle. The BSFC of HCCI engine is much better than that of original SI engine as shown in Figure 20b. The lower BSFC of HCCI engine might be caused by several reasons: (1) lower heat transfer loss from cylinder gas to the wall, (2) short combustion duration, and (3) lean mixture. The combustion duration of HCCI engine is much shorter than that of conventional SI engine. When the load increases (i.e., λ decreases in Figure 14a), the combustion phasing has to be retarded to avoid engine knocking as shown in Figure 14a.

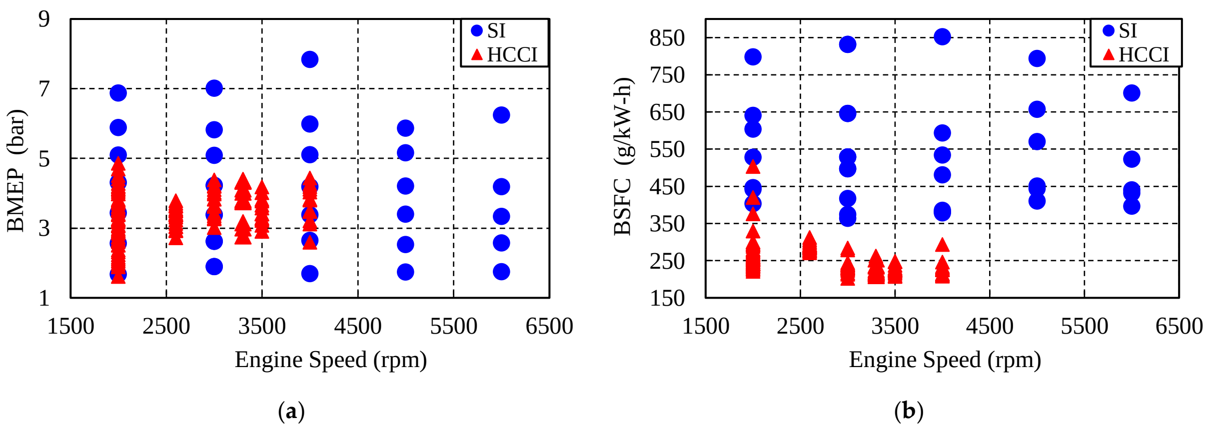

Figure 20. Comparison of engine characteristics between proposed HCCI and original SI engine: (**a**) BMEP; (**b**) BSFC.

The CO emission of HCCI engine is smaller than that of original SI engine (Figure 21a) due to the lean combustion. However, the HC emission is higher (Figure 21b) because of the low combustion temperature.

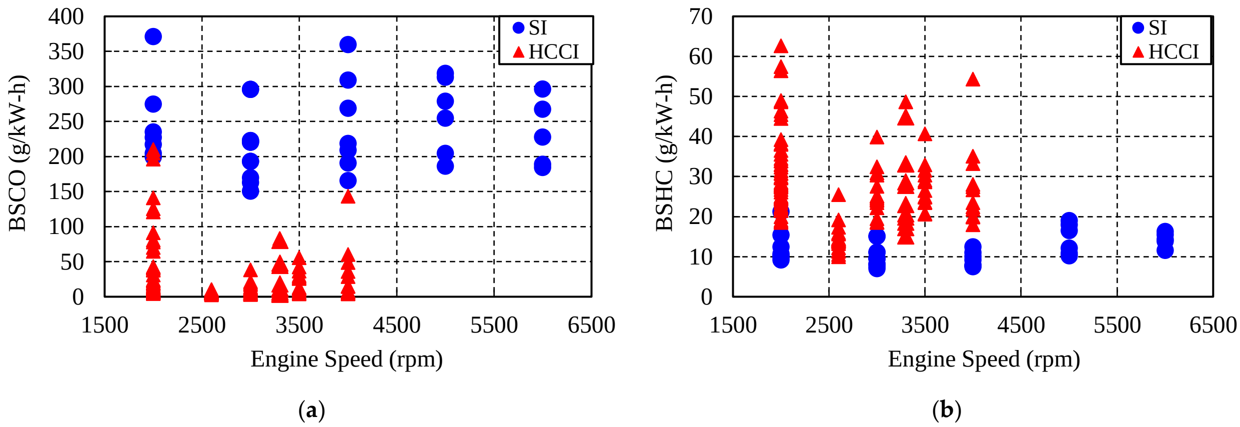

Figure 21. Comparison of exhaust emissions between proposed HCCI and original SI engine: (**a**) BSCO; (**b**) BSHC.

4. Conclusions

The proposed HCCI engine was operated with DME-gasoline dual-fuel in a conventional motorcycle engine. The engine test results and combustion analysis led to the following conclusions:

(1) To pursue both high engine output and low BSFC, the proposed HCCI system for a motorcycle engine is DME-gasoline dual-fuel with 25% EGR and $\lambda < 2$. Therefore, the design guide for HCCI engine obtaining high output and low BSFC can be led to a DME-gasoline dual-fuel system with suitable EGR ratio and air-fuel mixture not too lean.

(2) The maximum BMEP increase was from 2.93 to 4.86 bar, an increase of 65.8%, when the EGR was 0% to 25%. At 25% EGR, BMEP increased by 77.4% from 2.74 to 4.86 bar when the gasoline ratio increased from 0.13 to 0.35.

(3) The BSFC was improved great as compared with the original SI engine and NO emision was too small to measure.

(4) The thermal efficiency ranged from 30%–35% and had no clear relationship with λ or BMEP.

(5) Both BSCO and BSHC decreased when the exhaust temperature increased, whereas the exhaust temperature increased linearly with BMEP. When the exhaust temperature was > 550 K or BMEP was > 3.16 bar, the amount of CO emitted was very small.

(6) Both CA10 and CA50 were delayed by a decrease in λ. This is caused by the addition of more gasoline fuel, which delays combustion.

(7) The burn duration increased in line with λ because a leaner mixture causes slower combustion. The combustion efficiency was close to 100% when the burn duration was <10 deg CA.

To further improve the thermal efficiency of the proposed HCCI engine, future studies should modify the cooling system to reduce the cooling capacity.

Author Contributions: Y.-Y.W. designed the experiments; C.-T.J. performed the experiments and data reduction; Y.-Y.W. and C.-T.J. analyzed the data; Y.-Y.W. wrote the paper.

Funding: This research was funded by Ministry of Science and Technology (MOST, Taipei, Taiwan), grant number MOST 106-3113-E-027-002-CC2.X.

Acknowledgments: The authors would like to thank the Ministry of Science and Technology (MOST, Taipei, Taiwan) for their financial support. This manuscript was edited by Wallace Academic Editing.

Conflicts of Interest: The authors declare no conflict of interest. The founding sponsors had no role in the design of the study; in the collection, analyses, or interpretation of data; in the writing of the manuscript, and in the decision to publish the results.

Nomenclature

A	area of combustion chamber surface
BMEP	brake mean effective pressure
BSCO	brake-specific CO
BSFC	brake-specific fuel consumption
BSHC	brake-specific HC
BDC	bottom dead center
C_m	average piston speed
c_p	specific heat for constant pressure
CA	crank angle
CAD	crank angle degrees
CA10	crank angle at which the mass fraction burned is 10%
CA50	crank angle at which the mass fraction burned is 50%
CA90	crank angle at which the mass fraction burned is 90%
CO	carbon monoxide
CO_2	carbon dioxide
COV	coefficient of variation
DI	direct injection
DME	dimethyl ether
ECE	Economic Commission of Europe
EGR	exhaust gas recirculation
EPA	Environmental Protection Administration
FSN	filter smoke number
HC	hydrocarbons
HCCI	homogeneous charge compression ignition
HRR	heat release rate
H_2O_2	hydrogen peroxide
h	heat transfer coefficient
IMEP	indicated mean effective pressure
$IMEP_{avg}$	average IMEP
$IMEP_{std}$	standard deviation of IMEP
MFB	mass fraction burned
MHRR	maximum heat release rate
MRPR	maximum rate of pressure rise
NMHC	non-methane hydrocarbons
NO	nitric oxide
NO_x	nitrogen oxides
NVO	negative valve overlap
OBD	on-board diagnostics
OH	hydroxyl radical
P	cylinder gas pressure (bar)
PFI	port fuel injection
PM	particulate matter
Q_{LHV}	low heating value of fuel
RON	research octane number
S_t	Stanton number
SCR	selective catalytic reduction
SI	spark ignition
T	cylinder gas temperature
TDC	top dead center
V	cylinder volume
WMTC	worldwide motorcycle test cycle
bhp	brake horsepower

m_f	fuel mass supplied per cycle
λ	air–fuel equivalence ratio
θ	crank angle (degree)
γ	specific heat ratio
η_c	combustion efficiency (%)
η_f	fuel efficiency (%)
η_{th}	brake thermal efficiency (%)

References

1. Taiwan Ministry of Transportation and Communications (MOTC). Motor Vehicle Registration (Sept. 2018). Available online: http://stat.motc.gov.tw/mocdb/stmain.jsp?sys=100&funid=e3301 (accessed on 6 November 2018).
2. Lin, C.Y.; Wu, S.Y.; Liang, H.J.; Liu, Y.C.; Ueng, T.H. Metabolomic analysis of the effects of motorcycle exhaust on rat testes and liver. *Aerosol Air Qual. Res.* **2014**, *14*, 1714–1725. [CrossRef]
3. Chuang, S.C.; Chen, S.J.; Huang, K.L.; Chang-Chien, G.P.; Wang, L.C.; Huang, Y.C. Emissions of polychlorinated dibenzo-p-dioxin and polychlorinated dibenzofuran from motorcycles. *Aerosol Air Qual. Res.* **2010**, *10*, 533–539. [CrossRef]
4. Taiwan Environmental Protection Administration (EPA). Air Pollutant Emission Regulations for Transportation Vehicles. Available online: https://oaout.epa.gov.tw/law/LawContent.aspx?id=FL015347 (accessed on 6 November 2018).
5. Finesso, R.; Spessa, E.; Venditti, M.; Yang, Y. Offline and Real-Time Optimization of EGR ratio and Injection Timing in Diesel Engines. *SAE Int. J. Engines* **2015**, *8*, 2099–2119. [CrossRef]
6. Theis, J.; Kim, J.; Cavataio, G. TWC+LNT/SCR Systems for Satisfying Tier 2, Bin 2 Emission Standards on Lean-Burn Gasoline Engines. *SAE Int. J. Fuels Lubr.* **2015**, *8*, 474–486. [CrossRef]
7. De Abreu Goes, J.; Olsson, L.; Berggrund, M.; Kristoffersson, A.; Gustafson, L.; Hicks, M. Performance Studies and Correlation between Vehicle- and Rapid- Aged Commercial Lean NOx Trap Catalysts. *SAE Int. J. Engines* **2017**, *10*, 1613–1626. [CrossRef]
8. Lin, Y.C.; Yang, P.M.; Chen, C.B. Reducing emissions of polycyclic aromatic hydrocarbons and greenhouse gases from engines using a novel plasma-enhanced combustion system. *Aerosol Air Qual. Res.* **2013**, *13*, 1107–1115. [CrossRef]
9. Wei, M.; Nguyen, T.S.; Turkson, R.F.; Liu, J.; Guo, G. Water injection for higher engine performance and lower emissions. *J. Energy Inst.* **2017**, *90*, 285–299. [CrossRef]
10. Wu, Y.Y.; Chen, B.C.; Hwang, J.J.; Chen, C.Y. Performance and emissions of motorcycle engines using water–fuel emulsions. *Int. J. Veh. Des.* **2009**, *49*, 91–110. [CrossRef]
11. Hasan, M.M.; Rahman, M.M. Homogeneous charge compression ignition combustion: Advantages over compression ignition combustion, challenges and solutions. *Renew. Sustain. Energy Rev.* **2016**, *57*, 282–291. [CrossRef]
12. Agarwal, A.K.; Singh, A.P.; Maurya, R.K. Evolution, challenges and path forward for low temperature combustion engines. *Prog. Energy Combust. Sci.* **2017**, *61*, 1–56. [CrossRef]
13. Jung, D.; Iida, N. Thermal and chemical effects of the in-cylinder charge at IVC on cycle-to-cycle variations of DME HCCI combustion with combustion-phasing retard by external and rebreathed EGR. *Appl. Therm. Eng.* **2017**, *113*, 132–149. [CrossRef]
14. Mohebbi, M.; Reyhanian, M.; Hosseini, V.; Muhamad Said, M.F.; Aziz, A.A. The effect of diethyl ether addition on performance and emission of a reactivity controlled compression ignition engine fueled with ethanol and diesel. *Energy Convers. Manag.* **2018**, *174*, 779–792. [CrossRef]
15. Hasan, M.M.; Rahman, M.M.; Kadirgama, K.; Ramasamy, D. Numerical study of engine parameters on combustion and performance characteristics in an n-heptane fueled HCCI engine. *Appl. Therm. Eng.* **2018**, *128*, 1464–1475. [CrossRef]
16. Kalaskar, V.; Splitter, D.; Szybist, J. Gasoline-Like Fuel Effects on High-Load, Boosted HCCI Combustion Employing Negative Valve Overlap Strategy. *SAE Int. J. Fuels Lubr.* **2014**, *7*, 82–93. [CrossRef]
17. Yun, H.; Wermuth, N.; Najt, P. Extending the High Load Operating Limit of a Naturally-Aspirated Gasoline HCCI Combustion Engine. *SAE Int. J. Engines* **2010**, *3*, 681–699. [CrossRef]

18. Szybist, J.P.; Nafziger, E.; Weall, A. Load Expansion of Stoichiometric HCCI Using Spark Assist and Hydraulic Valve Actuation. *SAE Int. J. Engines* **2010**, *3*, 244–258. [CrossRef]
19. Lawler, B.; Lacey, J.; Güralp, O.; Najtc, P.; Filipi, Z. HCCI combustion with an actively controlled glow plug: The effects on heat release, thermal stratification, efficiency, and emissions. *Appl. Energy* **2018**, *211*, 809–819. [CrossRef]
20. Ji, C.; Dec, J.; Dernotte, J.; Cannella, W. Boosted Premixed-LTGC/HCCI Combustion of EHN-doped Gasoline for Engine Speeds Up to 2400 rpm. *SAE Int. J. Engines* **2016**, *9*, 2166–2184. [CrossRef]
21. Wang, Y.; Liu, H.; Huang, Z.; Liu, Z. Study on combustion and emission of a dimethyl ether-diesel dualfuel premixed charge compression ignition combustion engine with LPG (liquefied petroleum gas) as ignition inhibitor. *Energy* **2016**, *96*, 278–285. [CrossRef]
22. Pedersen, T.D.; Schramm, J.; Yanai, T.; Sato, Y. *Controlling the Heat Release in HCCI Combustion of DME with Methanol and EGR*; SAE Technical Paper; SAE International: Warrendale, PA, USA, 2010.
23. Li, G.; Zhang, C.; Zhou, J. Study on the knock tendency and cyclical variations of a HCCI engine fueled with n-butanol/n-heptane blends. *Energy Convers. Manag.* **2017**, *133*, 548–557. [CrossRef]
24. Khandal, S.V.; Banapurmath, N.R.; Gaitonde, V.N. Performance studies on homogeneous charge compression ignition (HCCI) engine powered with alternative fuels. *Renew. Energy* **2019**, *132*, 683–693. [CrossRef]
25. Zheng, Z.; Xia, M.; Liu, H.; Wang, X.; Yao, M. Experimental study on combustion and emissions of dual fuel RCCI mode fueled with biodiesel/n-butanol, biodiesel/2,5-dimethylfuran and biodiesel/ethanol. *Energy* **2018**, *148*, 824–838. [CrossRef]
26. Putrasari, Y.; Jamsran, N.; Lim, O. An investigation on the DME HCCI autoignition under EGR and boosted operation. *Fuel* **2017**, *200*, 447–457. [CrossRef]
27. Ito, S.; Ikeda, H.; Jung, D.W.; Iida, N. *Potential of Stratification Charge for Reducing Pressure-Rise Rate in HCCI Engines Based on Multi-Zone Modeling and Experiments by Using RCM*; SAE Technical Paper; SAE International: Warrendale, PA, USA, 2013.
28. Jamsran, N.; Lim, O.; Iida, N. *An Investigation on DME HCCI Engine about Combustion Phase Control Using EGR Stratification by Numerical Analysis*; SAE Technical Paper; SAE International: Warrendale, PA, USA, 2012.
29. Nishi, M.; Kanehara, M.; Iida, N. Assessment for innovative combustion on HCCI engine by controlling EGR ratio and engine speed. *Appl. Therm. Eng.* **2016**, *99*, 42–60. [CrossRef]
30. Lee, C.; Chung, J.; Lee, K. Emission Characteristics for a Homogeneous Charged Compression Ignition Diesel Engine with Exhaust Gas Recirculation Using Split Injection Methodology. *Energies* **2017**, *10*, 2146. [CrossRef]
31. Lee, K.; Cho, S.; Kim, N.; Min, K. A study on combustion control and operating range expansion of gasoline HCCI. *Energy* **2015**, *91*, 1038–1048. [CrossRef]
32. Szybist, J.P.; Edwards, K.D.; Foster, M.; Confer, K.; Moore, W. *Characterization of Engine Control Authority on HCCI Combustion as the High Load Limit is Approached*; SAE Technical Paper; SAE International: Warrendale, PA, USA, 2013.
33. Wu, Y.Y.; Chen, B.C.; Hsieh, F.C. Heat transfer model for small-scale air-cooled spark ignition four-stroke engines. *Int. J. Heat Mass Transf.* **2006**, *49*, 3895–3905. [CrossRef]
34. Wu, Y.Y.; Chen, B.C.; Wang, J.H. Experimental study on HCCI combustion in a small engine with various fuels and EGR. *Aerosol Air Qual. Res.* **2016**, *16*, 3338–3348. [CrossRef]
35. Mack, J.H.; Flowers, D.L.; Buchholz, B.A.; Dibble, R.W. Investigation of HCCI combustion of diethyl ether and ethanol mixtures using carbon 14 tracing and numerical simulations. *Proc. Combust. Inst.* **2005**, *30*, 2693–2700. [CrossRef]
36. Wu, Y.Y.; Jang, C.T.; Chen, B.L. Combustion characteristics of HCCI in motorcycle engine. *J. Eng. Gas Turbines Power-Trans. ASME* **2010**, *132*. [CrossRef]
37. Yao, M.; Chen, Z.; Zheng, Z.; Zhang, B.; Xing, Y. Study on the controlling strategies of homogeneous charge compression ignition combustion with fuel of dimethyl ether and methanol. *Fuel* **2006**, *85*, 2046–2056. [CrossRef]
38. Holman, J.P. *Experimental Methods for Engineers*, 5th ed.; McGraw-Hill: New York, NY, USA, 1989; ISBN 9780070296220.
39. Ceviz, M.A.; Kaymaz, I. Temperature and air-fuel ratio dependent specific heat ratio functions for lean burned and unburned mixture. *Energy Convers. Manag.* **2005**, *46*, 2387–2404. [CrossRef]

40. Sun, R.; Thomas, R.; Gray, C.L., Jr. *An HCCI Engine: Power Plant for a Hybrid Vehicle*; SAE Technical Paper; SAE International: Warrendale, PA, USA, 2004.
41. Fathi, M.; Saray, R.K.; Checkel, M.D. The Influence of Exhaust Gas Recirculation (EGR) on Combustion and Emissions of n-heptane/Natural Gas Fuelled Homogeneous Charge Compression Ignition (HCCI) Engines. *Appl. Energy* **2011**, *88*, 4719–4724. [CrossRef]
42. Wu, Y.Y.; Chen, B.C.; Wang, J.H. Application of HCCI Engine in Motorcycle for Emission Reduction and Energy Saving. *Aerosol Air Qual. Res.* **2015**, *15*, 2140–2149. [CrossRef]
43. Turns, S.R. *An Introduction to Combustion*, 3rd ed.; McGraw-Hill: Singapore, 2012; p. 172. ISBN 978-007-108687-5.
44. Sjöberg, M.; Dec, J.E. An investigation into lowest acceptable combustion temperatures for hydrocarbon fuels in HCCI engines. *Proc. Combust. Inst.* **2005**, *30*, 2719–2726. [CrossRef]
45. Machrafi, H.; Cavadias, S.; Amouroux, J. A parametric study on the emissions from an HCCI alternative combustion engine resulting from the auto-ignition of primary reference fuels. *Appl. Energy* **2008**, *85*, 755–764. [CrossRef]
46. Kelly-Zion, P.L.; Dec, J.E. A computational study of the effect of fuel type on ignition time in homogeneous charge compression ignition engines. *Proc. Combust. Inst.* **2000**, *28*, 1187–1194. [CrossRef]